Heterogeneous & Homogeneous & Bio- & Nano-
CHEMCATCHEM
CATALYSIS

# Accepted Article

**Title:** Ni/LnOx catalysts (Ln = La, Ce or Pr) for CO2 methanation

**Authors:** Virginia Alcalde-Santiago, Arantxa Davó-Quiñonero, Dolores Lozano-Castelló, Adrián Quindimil, Unai De-La-Torre, Beñat Pereda-Ayo, José A. González-Marcos, Juan R. González-Velasco, and Agustín Bueno López



**To be cited as:** *ChemCatChem* 10.1002/cctc.201801585

**Link to VoR:** http://dx.doi.org/10.1002/cctc.201801585

A Journal of
ChemPubSoc Europe

WILEY-VCH

www.chemcatchem.org

10.1002/cctc.201801585

WILEY-VCH

FULL PAPER

# Ni/LnOx catalysts (Ln = La, Ce or Pr) for $CO_2$ methanation

Virginia Alcalde-Santiago,[a] Arantxa Davó-Quiñonero,[a] Dolores Lozano-Castelló,[a] Adrián Quindimil,[b] Unai De-La-Torre,[b] Beñat Pereda-Ayo,[b] José A. González-Marcos,[b] Juan R. González-Velasco,[b] Agustín Bueno-López*,[a]

**Abstract:** The effect of the LnOx support has been studied for Ni-based $CO_2$ methanation catalysts. 10 wt. % nickel catalysts with LaOx, $CeO_2$ and PrOx supports have been prepared, characterized by $N_2$ adsorption, XRD, XRF, TG-MS ($N_2$-TPD and $H_2$-TPR) and XPS, and have been tested for $CO_2$ methanation. The catalytic activity follows the trend Ni/$CeO_2$ > Ni/PrOx >> Ni/LaOx, all catalysts being very selective towards $CH_4$ formation. The activity depends both on the nature of the catalytic active sites and on the stability of the surface $CO_2$ and $H_2O$ species. Ni/$CeO_2$ is the most active catalyst because (i) the $Ni^{2+}$-ceria interaction leads to the formation of the highest population of active sites for $CO_2$ dissociation, (ii) the reduced $Ni^0$ sites where $H_2$ dissociation takes place are the most electronegative and active, and (iii) the stability of surface $CO_2$ and $H_2O$ species is lowest. Ni/LaOx achieves lower activity because of the strong chemisorption of $H_2O$ and $CO_2$, which poison the catalyst surface, and because this support is not able to promote the formation of highly active sites for $CO_2$ and $H_2$ dissociation. The behavior of Ni/PrOx is intermediate, being slightly lower to that of Ni/$CeO_2$ because the formation of active sites is not so efficient and because the stability of chemisorbed $CO_2$ is slightly higher.

## Introduction

$CO_2$ methanation is known as the Sabatier reaction, because it was first reported by Paul Sabatier in the 1910s. This is an exothermic reaction between $CO_2$ and $H_2$ that yields $CH_4$ + $H_2O$. [1-5]

$CO_2 + 4H_2 \rightarrow CH_4 + 2H_2O \quad \Delta H = -165.0$ kJ/mol
Sabatier reaction (1)

Despite the reaction is known since more than 100 years ago, scientists are paying more attention to this process in the last decade[6-15] because it has been identified as a potential route to valorize $CO_2$ emissions, yielding a valuable fuel.
From an environmental point of view, the key aspect of this process is the utilization of $H_2$ obtained from renewable sources, [16-19] and this type of $H_2$ is expected to be available at low prize in a hypothetical energy scenario where $H_2$ is massively used as energy vector. $CH_4$ has several advantages in comparison to $H_2$ as energy vector. One of the most relevant is that can be liquefied and transported using the facilities already available for natural gas, while storage and transportation of $H_2$ are so far unsolved problems that will require an important economical inversion.
As a proof of concept, Hashimoto et al.[20] successfully built in 1996 a prototype plant at the Institute for Materials Research, at the Tohoku University in Japan, using electrolytic cells working on solar energy for $H_2O$ electrolysis and $H_2$ production. This $H_2$ was used for $CO_2$ methanation, and the $CH_4$ obtained was combusted in a reactor with a $CO_2$ capture unit, using this $CO_2$ for further methanation, thus closing the energy cycle without $CO_2$ emissions.
Despite the Sabatier reaction is exothermic, it has kinetic restrictions due to the high stability of the reactant gases, and a catalyst is necessary to accelerate the reaction until rates with practical relevance for industrial application. Several active phases have been studied, including ruthenium,[21-28] palladium,[29-31] rhodium[32-35] and nickel.[36-42] Noble metal catalysts are able to operate at lower temperature than nickel catalysts, but the prize of noble metals is much higher and nickel catalysts are a promising option for mild temperature.
$CO_2$ methanation nickel catalysts have been studied using different supports, and the most studied are alumina,[8, 10, 15, 37, 39-41] pure ceria,[10] ceria-zirconia mixed oxides,[11, 39] silica,[12] titania[10] and zirconia[38] among others.[43-45] The role of the support in the catalytic activity has been related with the dispersion of nickel, with the influence in the reducibility of the nickel oxide species due to the metal-support interaction and with the $CO_2$ chemisorption capacity.[43]
Despite alumina is the most studied support, there are evidences of the higher catalytic activity of nickel catalysts with ceria-based supports.[10, 39] It has been reported that alumina-supported nickel catalysts suffer from severe carbon deposition and poor stability due to the high reaction temperature.[43] This high catalytic activity of Ni/$CeO_2$ has motivated us to focus our research on the behavior of different Ni/LnOx catalysts, comparing different LnOx supports and understanding the role of the support in the catalytic performance.
In order to evaluate the catalytic activity of Ni catalysts using lanthanide oxide supports, the goals of the present study have been to prepare, characterize and test the catalytic activity for $CO_2$ methanation of nickel catalysts with LaOx, $CeO_2$ and PrOx supports, paying attention to the main features of the LnOx support affecting the catalytic activity. LaOx and PrOx oxides have been selected to be compared with $CeO_2$ because they have some interesting properties for the Sabatier reaction. LaOx is more basic than $CeO_2$, and therefore is expected to improve $CO_2$ and $H_2O$ chemisorption. However, La can hardly accomplish redox cycles while Ce and Pr can do. On the other hand, Ce and Pr chemistry is similar in many aspects, since both elements can adopt 3+ and 4+ oxidation states, but the redox and

[a] Ms.V. Alcalde-Santiago, Ms. A. Davó-Quiñonero, Prof. Dr. Dolores Lozano-Castelló, and Prof. Dr. A. Bueno-López. Department of Inorganic Chemistry. University of Alicante. Carretera de San Vicente s/n. E03080, Alicante (Spain). *agus@ua.es

[b] Mr. A. Quindimil, Dr. U. De-La-Torre, Dr. B. Pereda-Ayo, Prof. Dr. J. A. González-Marcos and Prof. Dr. J. R. González-Velasco. Departamento de Ingeniería Química, Facultad de Ciencia y Tecnología, Universidad del País Vasco, UPV/EHU, Campus de Leioa, P. O. Box 644, ES-48080 Bilbao, Bizkaia, Spain

Supporting information for this article is given via a link at the end of the document.

chemisorption properties are slightly different. This set of materials will be useful to identify the importance of the different steps of the reaction mechanisms (chemisorption and redox steps) and the role of the support in the behavior of the nickel catalysts.

## Results and Discussion

2.1. Fresh catalysts and supports characterization by $N_2$ adsorption.

Three catalysts have been prepared and characterized in this study, which are referred to as $Ni/CeO_2$, Ni/PrOx and Ni/LaOx. Details about the preparation procedure are included in the experimental section at the end of this document. Figure 1 shows the $N_2$ physisorption isotherms of the fresh supports and catalysts, and the specific surface areas are compiled in Table 1.

**Table 1.** Specific surface area and nickel content.

| | BET ($m^2/g$) | Ni (wt. %) |
|---|---|---|
| $CeO_2$ | 12 | - |
| $PrO_x$ | 3 | - |
| $LaO_x$ | 4 | - |
| $Ni/CeO_2$ | 9 | 10.6 ± 0.7 |
| $Ni/PrO_x$ | 13 | 10.7 ± 0.9 |
| $Ni/LaO_x$ | 13 | 9.3 ± 0.5 |

The specific surface areas are low for all supports and catalysts (≤ 13 $m^2/g$), as expected for lanthanide oxides prepared by calcination of citrates. However, all catalysts present similar surface areas, and this allows comparison of the catalytic results ruling out differences in the specific surface areas. The $N_2$ physisorption isotherms present very low $N_2$ adsorption at low relative pressures due to the very low microporosity, and hysteresis loops that suggest the presence of large mesopores or even macroporosity. Meso and macropores could be attributed to the interparticles space, and the absence of micropores suggests that particles have not internal pores. Note that the surface areas of PrOx and LaOx increase upon nickel loading, and as it will be demonstrated in the next section, this can be attributed to changes in the crystalline phases of the supports after nickel impregnation.

2.2. Fresh catalysts and supports characterization by XRD and XRF.

The nickel percentage on the catalysts was determined by XRF, and the results obtained are included in Table 1. The nickel contents are near the target value of 10 wt. %, as expected.

Figure 2 shows the X-ray diffractograms for the supports and catalysts, and the nature of the crystalline phases is different for each material. The $Ni/CeO_2$ catalyst shows the characteristic peaks of $CeO_2$ (JCPDS 00-034-0394) and NiO (JCPDS 01-075-0269), while the bare support only shows the characteristic peaks of $CeO_2$ (Figure 2a), as expected. Different crystalline parameters were determined from the diffractograms of Figure 2a, which are compiled in Table 2.

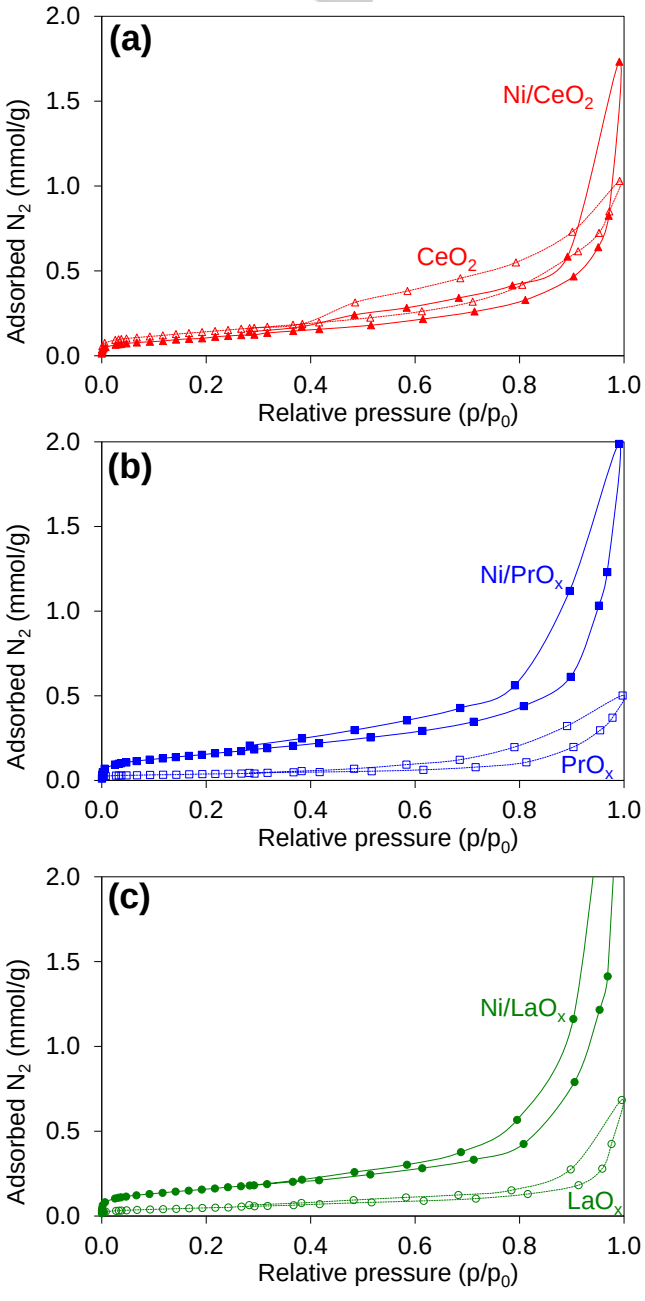


**Figure 1.** $N_2$ physisorption isotherms at -196 ºC of fresh catalysts and supports. (a) $CeO_2$, (b) PrOx and (c) LaOx samples.

**Table 2.** Crystalline parameters determined from XRD for $CeO_2$ and $Ni/CeO_2$.

| | Cell parameter $CeO_2$ (nm) | Crystallite size of $CeO_2$ (nm) | Crystallite size of NiO (nm) | $Ni^{2+}$ inserted into the $CeO_2$ lattice (%) |
|---|---|---|---|---|
| $CeO_2$ | 0.5425 | 20 | - | - |
| $Ni/CeO_2$ | 0.5415 | 31 | 22 | 1.4 |

The cell parameter of bare $CeO_2$ is 0.5425 nm, and this cell parameter decreases slightly to 0.5415 nm upon NiO loading. Note that these values are quite similar to that reported on the JCPDS database for this material (0.5411 nm). The small contraction of the unit cell after NiO loading could be attributed to the insertion of nickel cations into the ceria lattice, since nickel cations are smaller (0.078 nm for $Ni^{2+}$ and 0.062 nm for $Ni^{3+}$) than $Ce^{4+}$ cations (0.097 nm). The difference between the cell parameters of $CeO_2$ and $Ni/CeO_2$ has been used to estimate, using the Kim's equation,[46, 47] the amount of $Ni^{2+}$ inserted into the ceria lattice. This equation can be written as follows:

CP ($Ni^{2+}$-doped $CeO_2$) = CP ($CeO_2$) – (0.022·($rNi^{2+}$ + $rCe^{4+}$) + 0.00015·($ZNi^{2+}$ - $ZCe^{4+}$) ·XNi
Kim's reaction (2)

where CP means cell parameter, $rNi^{2+}$ and $rCe^{4+}$ are the cationic radii of $Ni^{2+}$ and $Ce^{4+}$ respectively, $ZNi^{2+}$ and $ZCe^{4+}$ are the cationic charges of $Ni^{2+}$ and $Ce^{4+}$ respectively, and XNi is the fraction of $Ni^{2+}$ inserted into the parent ceria lattice.

These calculations predict that the percentage of $Ni^{2+}$ inserted into the $CeO_2$ lattice in the $Ni/CeO_2$ catalyst amounts to 1.4 %, which is much lower than the total amount of nickel in the catalyst. Therefore, these XRD results indicate that most nickel is not forming a solid solution, but is present as a segregated phase.
The crystallite sizes estimated for $CeO_2$, using the Scherrer equation and the (111) plane at 2θ = 28.5º, are 20 and 31 nm for the support and catalyst, respectively, and the size of NiO crystallites (estimated with the (200) plane at 2θ = 43.3º) is 22 nm, that is, the sizes of $CeO_2$ and NiO crystallites are of the same magnitude order. Note that the size of $CeO_2$ slightly increases upon nickel doping, and this could be due to the promoting effect towards sintering of the $Ni^{2+}$ cations inserted into the ceria lattice.[48]
The diffractograms of the praseodymia samples are included in Figure 2b, and some crystalline parameters determined from these diffractograms are compiled in Table 3.

**Table 3.** Crystalline parameters determined from XRD for PrOx and Ni/PrOx .

| | Cell parameter $Pr_6O_{11}$ (nm) | Crystallite size of $Pr_6O_{11}$ (nm) |
|---|---|---|
| PrOx | 0.5459 | 26 |
| Ni/PrOx | 0.5462 | 26 |

The bare PrOx support shows a diffractogram consistent with the presence of the $Pr_6O_{11}$ phase (JCPDS 00-042-1121), and the tiny shoulder in the peak at 2θ = 47.3º suggests the presence of few $PrO_2$ (JCPDS 00-024-1006). The Ni/PrOx catalyst also shows peaks of these two phases, but the formation of the $PrO_2$ phase is promoted upon nickel loading. Peaks of NiO are not clearly shown in the Ni/PrOx diffractogram, and only a very broad band that could be assigned to this phase is observed at 2θ = 43.3 º. The cell parameters of the $Pr_6O_{11}$ phase were estimated to evaluate if $Ni^{2+}$ cations were inserted into the $Pr_6O_{11}$ phase or if well dispersed NiO crystals, with low diffraction capacity, were formed. The cell parameters calculated for the $Pr_6O_{11}$ phase were 0.5459 and 0.5462 nm for the PrOx and Ni/PrOx samples, respectively, and these values suggest that $Ni^{2+}$ cations were not inserted into the $Pr_6O_{11}$ phase because there is not cell contraction upon nickel loading. Therefore, it is postulated that small nickel oxide particles are probably spread on the PrOx support.

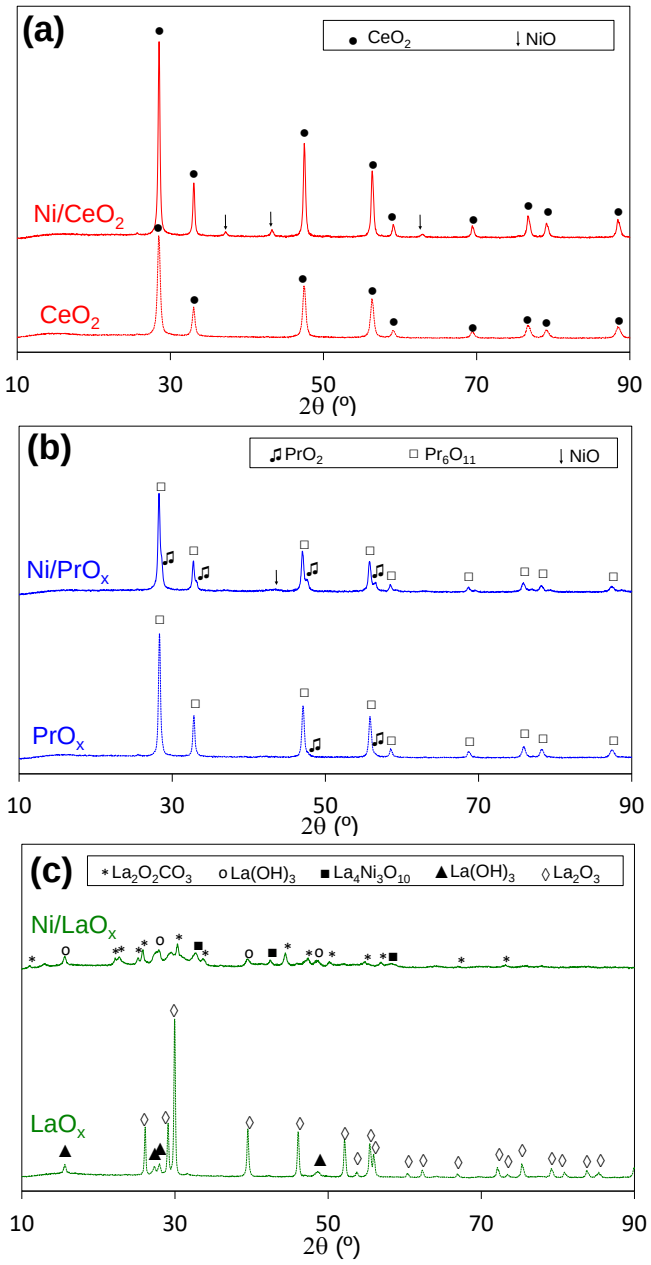


**Figure 2.** X-Ray diffractograms of fresh catalysts and supports. (a) $CeO_2$, (b) PrOx and (c) LaOx samples.

The diffractograms of the lanthanum samples (Figure 2c) are more complex than those of ceria and praseodymia. The LaOx support shows diffraction peaks of $La_2O_3$ (JCPDS 00-005-0602) and $La(OH)_3$ (JCPDS 00-036-1481), and these phases are partially modified upon nickel loading. The Ni/LaOx catalyst also shows peaks of the $La(OH)_3$ phase, but not those of $La_2O_3$, and instead, peaks of $La_2O_2(CO_3)$ (JCPDS 01-084-1963) and $La_4Ni_3O_{10}$ (JCPDS 01-083-1164) are identified. In this case, NiO peaks are not detected. The formation of lanthanum carbonates after impregnation of lanthana with metal salts was already reported by Bernal et al.[49, 50] and was attributed to the basic character of this oxide. Huanling et al. also reported the formation of $La_2O_2(CO_3)$ on a Ni/$La_2O_3$ $CO_2$ methanation catalyst. [44]

In conclusion, the XRD characterization evidences important differences in the interaction between nickel and the LnOx supports. The Ni/$CeO_2$ catalyst consists of a mixture of NiO and $CeO_2$ nanoparticles with average crystallite sizes of 22 and 30 nm, respectively, and a few fraction of nickel cations inserted into the $CeO_2$ lattice. The Ni/PrOx catalyst combines a high proportion of the $Pr_6O_{11}$ phase mixed with a lower proportion $PrO_2$, and nickel oxide particles are probably dispersed on these phases forming small particles with low crystallinity and without evidences of nickel cations insertion into the PrOx lattices. Finally, the Ni/LaOx catalyst combines lanthanum hydroxide with partially carbonated oxides, and nickel forms a Ni-La mixed oxide. Evidences of the presence of NiO particles were not obtained from the Ni/LaOx diffractogram, but the presence of small nickel oxide particles with low crystallinity cannot be ruled out.

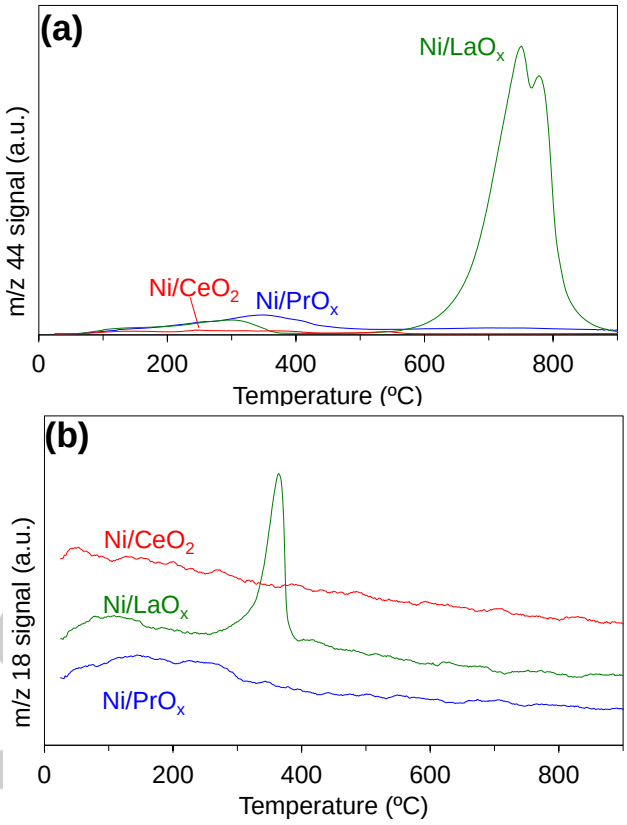


**Figure 3.** Characterization of fresh catalysts by Temperature Programmed Desorption in a $N_2$ flow followed by TG-MS. (a) $CO_2$ profiles (m/z 44 signal) and (b) $H_2O$ profiles (m/z 18 signals).

2.3. Fresh catalysts characterization by TG-MS ($N_2$-TPD and $H_2$-TPR experiments).

The catalysts were characterized by Temperature Programmed Desorption in $N_2$ and Reduction in $H_2$/Ar, and results are included in Figures 3 and 4 respectively.

The release of $CO_2$ (Figure 3a) and $H_2O$ (Figure 3b) under inert gas flow is highest for Ni/LaOx, and this is in agreement with the presence of $La(OH)_3$ and $La_2O_2(CO_3)$ observed by XRD (Figure 2c). $H_2O$ is released from Ni/LaOx around 350 ºC, and most $CO_2$ around 750 ºC, and this indicates that carbonate species are more stable than hydroxides.

The release of $H_2O$ from Ni/PrOx and Ni/$CeO_2$ is negligible (Figure 3b), while Ni/LaOx shows a $H_2O$ release peak between 300 and 400 ºC. In the same line, $CO_2$ is mainly emitted by Ni/LaOx above 600 ºC, and additionally, very few $CO_2$ is evolved from all catalysts in the 100-500 ºC range (Figure 3a). In this range of temperatures, the highest amount of $CO_2$ released comes from Ni/PrOx and the lowest from Ni/$CeO_2$.

As it will be discussed afterwards, the stability of the $H_2O$ and $CO_2$ species on the catalysts plays an important role during the catalytic methanation of $CO_2$, as $CO_2$ is one of the reactants and $H_2O$ is one of the reaction products.

The reduction of the catalysts in $H_2$-TPR experiments also provides valuable information to explain their catalytic behavior.

The Ni/$CeO_2$ catalyst (Figure 4a) shows a $H_2O$ peak around 370 ºC that can be attributed to the reduction of $Ni^{2+}$ to $Ni^0$. Quantitative calculations were performed using the area under the peak and a reference CuO sample, and the consumption of $H_2$ exactly matches the amount required for 100 % reduction of $Ni^{2+}$ to $Ni^0$ (Table 4). This confirms that the amount of Ni on the Ni/$CeO_2$ catalyst is 10 %, and that probably all nickel is present on the fresh catalyst as $Ni^{2+}$ cations.

**Table 4.** Estimation from $H_2$ consumption in $H_2$-TPR experiments of the percentage of nickel reduced assuming the presence of $Ni^{2+}$ or $Ni^{3+}$ cations on the catalysts.

| | $Ni^{2+}$ reduced (%) | $Ni^{3+}$ reduced |
|---|---|---|
| Ni/$CeO_2$ | 100 | 66 |
| Ni/PrOx | 205 | 137 |
| Ni/LaOx* | 192 | 128 |

*The amount of $H_2O$ released from this catalyst in the $N_2$-TPD experiment has been subtracted for these calculations.

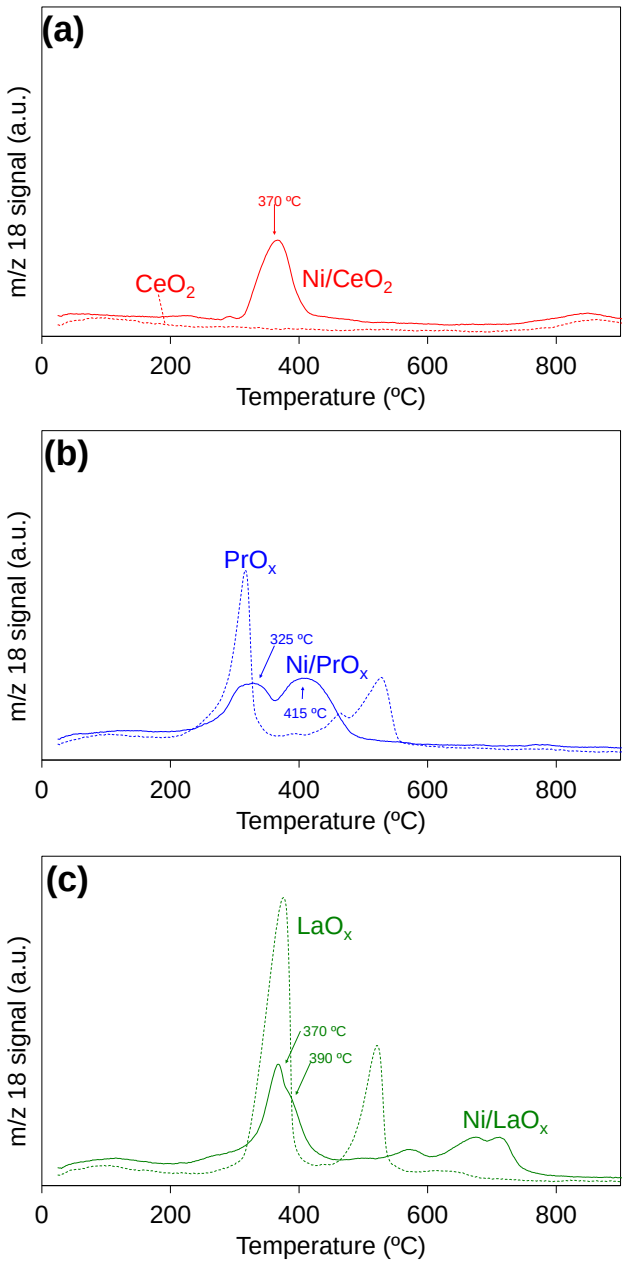


**Figure 4**. Characterization of fresh catalysts and supports by Temperature Programmed Reduction in a 5%$H_2$/Ar flow followed by TG-MS. (a) $CeO_2$, (b) PrOx and (c) LaOx.

The reduction of the $CeO_2$ support is not relevant under these experimental conditions. Only a small reduction peak is observed above 800 ºC that can be related with the reduction of bulk ceria. The null surface ceria reduction, which usually occurs around 400 ºC,[33, 51, 52] is consistent with the very low surface area of this catalyst (Table 1).

The $H_2$-TPR profile of Ni/PrOx (Figure 4b) shows a double peak in the 250-500 ºC range, with maxima at 325 and 415 ºC. From the area under this double peak, it is estimated that the consumption of $H_2$ is two times the amount required to reduce all nickel on the catalyst, assuming the presence of $Ni^{2+}$, and 1.4 times the amount required if $Ni^{3+}$ is assumed (Table 4). These calculations evidence that $Pr^{4+}$ cations are also reduced in this wide double peak. Note that XRD suggests the presence of $Ni^{2+}$ cations, and probably this is the main oxidation state of Ni cations. However, calculations for $Ni^{3+}$ have been also included to make sure there is a stoichiometric excess of $H_2$ consumed even if some $Ni^{3+}$ were present on the sample. Experimental evidences suggest that this is not the case, but it cannot be ruled out.

The $H_2$-TPR profile of Ni/LaOx is shown in Figure 4c, and several $H_2O$ release peaks are identified. The most intense peak appears at 370 ºC, but the release of $H_2O$ continues until 750 ºC with several smaller peaks and shoulders. Considering the conclusions of the XRD characterization, it is postulated that $H_2O$ released in the lowest temperature peak could be related with the reduction of nickel oxide, and the release at higher temperatures with the reduction of the Ni-La mixed oxide. Note that the release of $H_2O$, in this case, not only comes from the reduction of the catalyst by $H_2$, but also from the decomposition of $La(OH)_3$, as observed in $N_2$-TPD experiments (Figure 3b). The consumption of $H_2$ has been estimated from the Ni/LaOx profile in Figure 4c, subtracting the amount of $H_2O$ resealed due to $La(OH)_3$ decomposition, and this amount is two times higher than that required for all nickel reduction assuming the presence of $Ni^{2+}$ cations, and 1.3 times higher the amount required for $Ni^{3+}$ reduction (Table 4). It is hard to assume in this case the reduction of $La^{3+}$ cations, despite the LaOx support also shows two important $H_2O$ peaks in the $H_2$-TPR profiles (Figure 4c). Thus, it is tentatively proposed that the additional release of $H_2O$ might come from the reduction of hydroxyl or oxygen groups that are stable under $N_2$-TPD conditions but not in the presence of $H_2$.

The profiles on Figure 4 and calculations on Table 4 allows concluding that total reduction of the cationic nickel species present in all catalysts occurs during the $H_2$-TPR experiments, and that, in some cases, the support is also partially reduced together with the nickel reduction. The reduction temperature of nickel is around 370 ºC for all catalysts, but it is difficult to report a convincing reducibility trend for the catalysts due to overlapping of different events. In the case of Ni/LaOx, it must be taken into account that a fraction of nickel is reduced at much higher temperature (until 750 ºC) due to the formation of a Ni-La mixed oxide.

### 2.4. Catalytic methanation of $CO_2$.

Figure 5 shows catalytic results obtained with the Ni/LnOx catalysts, including the conversion of $CO_2$ (Figure 5a) and the carbon species distribution, $H_2$ conversion and selectivity to $CH_4$ and CO (Figure 5b).

The three $CO_2$ conversion curves are qualitatively similar, increasing with temperature until the thermodynamic equilibrium limits conversion at high temperature. The dashed curve in Figure 5a represents the theoretical maximum conversion at equilibrium with temperature, for the actual feed composition ($CO_2$/$H_2$/He = 1/4/1.25) and considering in calculations both $CO_2$ methanation and reverse water gas shift (RWGS, Equation 3) reactions.

$CO_2 + H_2 \rightarrow CO + H_2O$ $\Delta H = 41.2$ kJ/mol RWGS (3)

The onset temperature for $CO_2$ consumption is around 250 ºC for $Ni/CeO_2$ and Ni/PrOx and 275 ºC for Ni/LaOx, and the temperature required for 50% $CO_2$ conversion (T50) is 300, 312 and 365 ºC for $Ni/CeO_2$, Ni/PrOx and Ni/LaOx, respectively. These behaviors lead to the following catalytic trend:

$Ni/CeO_2$ > Ni/PrOx >> Ni/LaOx.

Concentrations of $H_2$ and $CO_2$ gases were independently determined by chromatographic analysis, and the $H_2$ conversion (data in Figure 5b) follow the same trend than $CO_2$ conversions (Figure 5a). However, due to the different stoichiometry and selectivity of reactions (1) and (3), the $H_2$ conversions are slightly lower than the corresponding $CO_2$ conversion.

$CH_4$ selectivity was almost 100 % in most experimental conditions, and only few CO was detected at 300 °C and above this temperature mainly for Ni/LaOx (Figure 5b). The balance of carbon between reactants and products of reaction was well closed in all experiments, thus ruling out carbon deposition on the catalysts. This hypothesis was confirmed in a experiment carried out with the $Ni/CeO_2$ catalyst at 350 and 300 °C for 24 h (Figure 1SM). After the reaction at 300 ºC, the used catalyst was submitted to a thermogravimetric analysis under 5% $O_2$/He, ruling out carbon deposition on the catalyst during reaction.

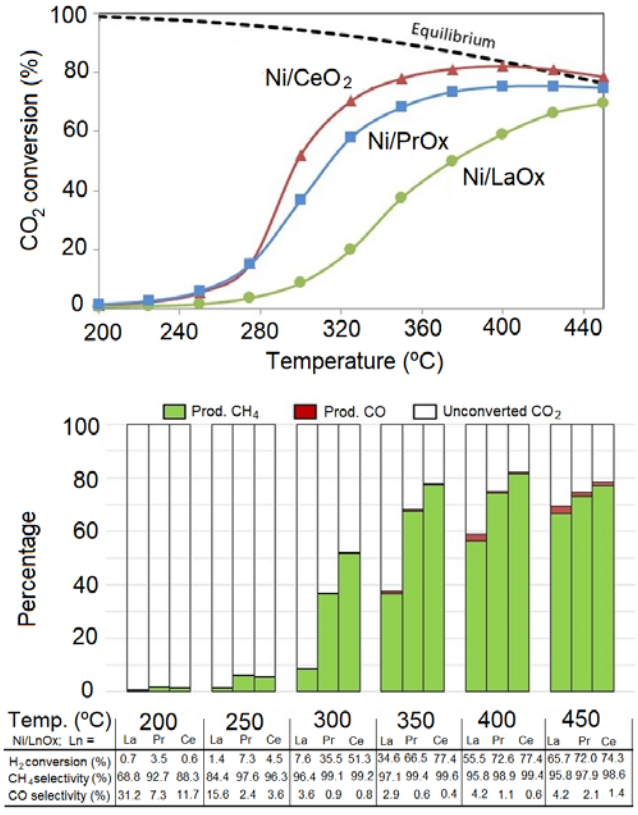


| Temp. (ºC) | 200 | | | 250 | | | 300 | | | 350 | | | 400 | | | 450 | | |
|---|---|---|---|---|---|---|---|---|---|---|---|---|---|---|---|---|---|---|
| Ni/LnOx: Ln = | La | Pr | Ce | La | Pr | Ce | La | Pr | Ce | La | Pr | Ce | La | Pr | Ce | La | Pr | Ce |
| $H_2$ conversion (%) | 0.7 | 3.5 | 0.6 | 1.4 | 7.3 | 4.5 | 7.6 | 35.5 | 51.3 | 34.6 | 66.5 | 77.4 | 55.5 | 72.6 | 77.4 | 65.7 | 72.0 | 74.3 |
| $CH_4$ selectivity (%) | 68.8 | 92.7 | 88.3 | 84.4 | 97.6 | 96.3 | 96.4 | 99.1 | 99.2 | 97.1 | 99.4 | 99.6 | 95.8 | 98.9 | 99.4 | 95.8 | 97.9 | 98.6 |
| CO selectivity (%) | 31.2 | 7.3 | 11.7 | 15.6 | 2.4 | 3.6 | 3.6 | 0.9 | 0.8 | 2.9 | 0.6 | 0.4 | 4.2 | 1.1 | 0.6 | 4.2 | 2.1 | 1.4 |

**Figure 5**. Catalytic methanation of $CO_2$. (a) $CO_2$ conversion and (b) carbon species distribution, $H_2$ conversion and selectivity to $CH_4$ and CO. (Experimental conditions were 16% $CO_2$ + 64% $H_2$ with He balance; 12000 $h^{-1}$).

Considering the characterization reported until now, the lowest activity of Ni/LaOx can be attributed to the nature of the nickel species and to the strong interaction of $CO_2$ and $H_2O$ with this catalyst. It has been reported that $H_2$ dissociates on reduced nickel sites, and dissociated H atoms further hydrogenate the surface carbon intermediates.[53] As it was observed by XRD, part of the nickel on the Ni/LaOx catalyst is conforming a Ni-La mixed oxide ($La_4Ni_3O_{10}$) with poor reducibility (750 ºC is required for total reduction in $H_2$-TPR conditions). On the contrary, the reducibility of all nickel species on $Ni/CeO_2$ and Ni/PrOx is much higher, being reduced around 370 ºC under $H_2$-TPR conditions. Therefore, it is expected that the formation under reaction conditions of reduced nickel sites suitable for $H_2$ dissociation is easier on $Ni/CeO_2$ and Ni/PrOx than on Ni/LaOx.

Additionally, $N_2$-TPD experiments showed that Ni/LaOx retains $CO_2$ and $H_2O$ strongly, while not $Ni/CeO_2$ and Ni/PrOx. Therefore, poisoning of the Ni/LaOx surface by these species is expected under $CO_2$ methanation conditions. In this context, it must be distinguished between the roles of $CO_2$ and $H_2O$ in the reaction mechanism. $H_2O$ is a reaction product that must be released from the catalyst surface once formed, and the onset temperature for $H_2O$ release from Ni/LaOx in $N_2$-TPD conditions is 250 ºC (Figure 3b). This is also the onset temperature for $CO_2$ methanation by Ni/LaOx (Figure 5a), that is, it seems that $CO_2$ methanation by Ni/LaOx only starts once the temperature is high enough for the desorption of $H_2O$ formed as a reaction product. On the contrary, $CO_2$ is a reactant gas, and there exist different opinions about the reaction pathway for $CO_2$ chemisorption and dissociation.[53] Two mechanisms have been proposed, which are referred to as associative and dissociative. In the associative mechanism, $CO_2$ is chemisorbed without dissociation, and then is hydrogenated in two consecutive steps removing one oxygen per step. In the dissociative mechanism, the $CO_2$ molecule is chemisorbed dissociativelly, providing a surface oxygen atom and a surface carbonyl. It has been proposed for ceria catalysts[33, 53] that reduced cerium cations ($Ce^{3+}$) are the active sites for chemisorption and dissociation of $CO_2$, and for this reason ceria favors the dissociative mechanism. The $Ce^{3+}$ sites are oxidized to $Ce^{4+}$ upon $CO_2$ dissociation, and must be reduced again by $H_2$ to close the redox cycle. This 3+/4+ redox cycle described for ceria is expected to occur also on praseodymia, because praseodymium is also able to adopt the 3+ and 4+ oxidation steps. However, lanthanum is not able to get involved in redox cycles because only forms 3+ cations.

The poor reducibility of nickel and the strong interaction of $CO_2$ and $H_2O$ with the catalyst explain the lower catalytic activity of Ni/LaOx, but differences between the catalytic behavior of $Ni/CeO_2$ and Ni/PrOx are not easily explained with the characterization results discussed until now, and the fresh and used catalysts were characterized by XPS to get further insight on these differences.

2.5. XPS characterization of the fresh and used catalysts.

The fresh and used catalysts were characterized by XPS, and the binding energy of the electrons was studied in three energy regions corresponding to the Ni2p, O1s and C1s transitions. Proper Ni2p profiles were obtained with $Ni/CeO_2$ and Ni/PrOx, but unfortunately, the La3d transition overlaps in this energy region, and it is not possible to obtain information about nickel in the Ni/LaOx catalyst by this technique. XPS characterization in the energy region of La3d transition is included in the supplementary material for the fresh and used Ni/LaOx catalyst (Figure 1SM).

The surface composition of the catalysts has been determined, and Table 4 shows the Ni/Ln atomic ratios.

The amount of surface nickel is higher on fresh $Ni/CeO_2$ than on fresh Ni/PrOx, and this is in agreement with the NiO peaks observed by XRD. The Ni/Ln ratio decreases after the catalytic tests for both catalysts, and this could be related with the decoration of the nickel particles with the NlOx support. This decoration has been reported for $Ni/CeO_2$ catalysis under reducing conditions, and has been observed that the decoration process is reversible.[54]

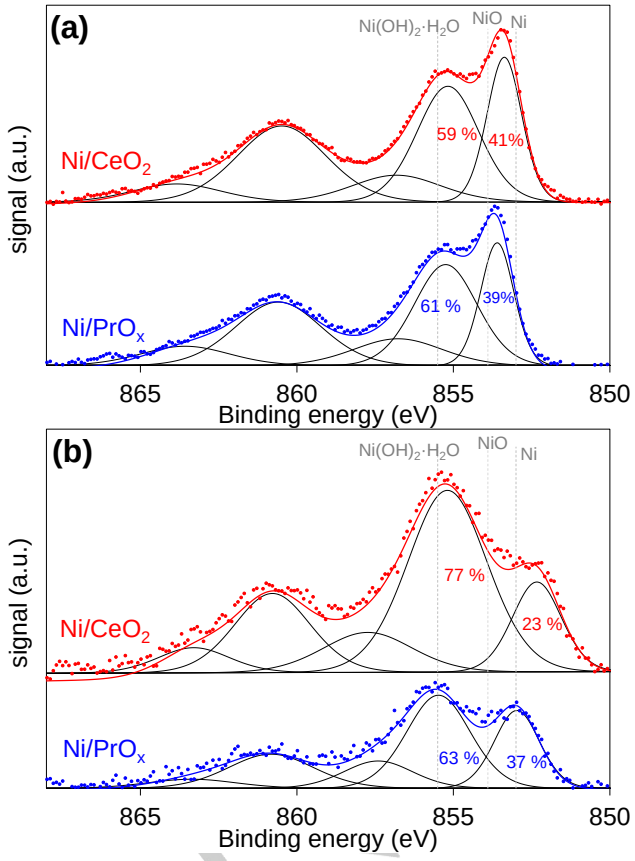


**Figure 6**. XPS characterization in the energy region of Ni2p transition for (a) fresh catalysts and (b) used catalysts.

Figure 6 shows the profiles in the Ni2p region. Assignation of bands in the Ni2p spectra is still a matter of debate, but it has been proposed[55-58] that the nature of the nickel species can be inferred from the position of the most intense peak. Auxiliary lines have been plotted in Figure 6 on particular energies reported in the literature for selected nickel species.[54-57] The main band in all spectra of Figure 6 can be deconvoluted in two contributions, suggesting the presence of nickel species of different nature. The position of these bands in the fresh catalysts confirms the presence of cationic species of nickel, probably NiO and $Ni(OH)_2{\cdot}H_2O$, and the presence of reduced nickel on fresh catalysts is ruled out.

The nature of the nickel species changes during the catalytic tests, as deduced from the XPS spectra of the used catalysts (Figure 6b). Part of the nickel species appear also oxidized after the catalytic tests and part are reduced to metal nickel. Considering the $H_2$-TPR characterization (Figure 4), nickel oxides are expected to be fully reduced to metal nickel during the reducing pre-treatment performed before the catalytic tests, and the presence of oxidized nickel species after the catalytic tests must be attributed to the redox process occurring during the methanation reaction, $CO_2$ being the oxidizing gas. It has to be mentioned that partial re-oxidation during atmospheric exposition cannot be ruled out.

One important conclusion from spectra in Figure 6 is that the binding energy of the metal nickel band is lower for $Ni/CeO_2$ than for Ni/PrOx, and this suggests that the interaction of metal nickel with the support is stronger on Ni/PrOx than on $Ni/CeO_2$, in agreement with the XRD characterization. It has been proposed that $H_2$ dissociation takes place on reduced nickel sites,[53] and therefore, it is reasonable to think that the higher negative charge density observed by XPS (Figure 6b) for reduced nickel on $Ni/CeO_2$ with regard to Ni/PrOx, is positive for $H_2$ dissociation. Therefore, it can be postulated that one of the reasons of the higher $CO_2$ methanation activity of $Ni/CeO_2$ with regard to Ni/PrOx is the presence of reduced nickel sites with higher activity for $H_2$ dissociation.

In the previously described dissociative mechanism,[53] $CO_2$ is chemisorbed on the reduced sites of the catalyst providing an oxygen atom and a metal carbonyl, which would explain the presence of cationic species of nickel formed with oxygen coming from $CO_2$. The used $Ni/CeO_2$ catalyst shows the highest concentration of oxidized nickel sites (Figure 6b), which can be related with $CO_2$ dissociation. The higher concentration of active sites for $CO_2$ dissociation could be another argument to explain the highest activity of $Ni/CeO_2$.

Additional information is obtained from the O1s spectra (Figure 7), which can be deconvoluted in three bands. Despite assignation of these bands is not easy, important differences are noticed in the band around 529 eV. This is the band with the lowest binding energy, that is, it belongs to the oxygen species with the highest negative charge density, which are expected to be those with the strongest interaction with metal cations.

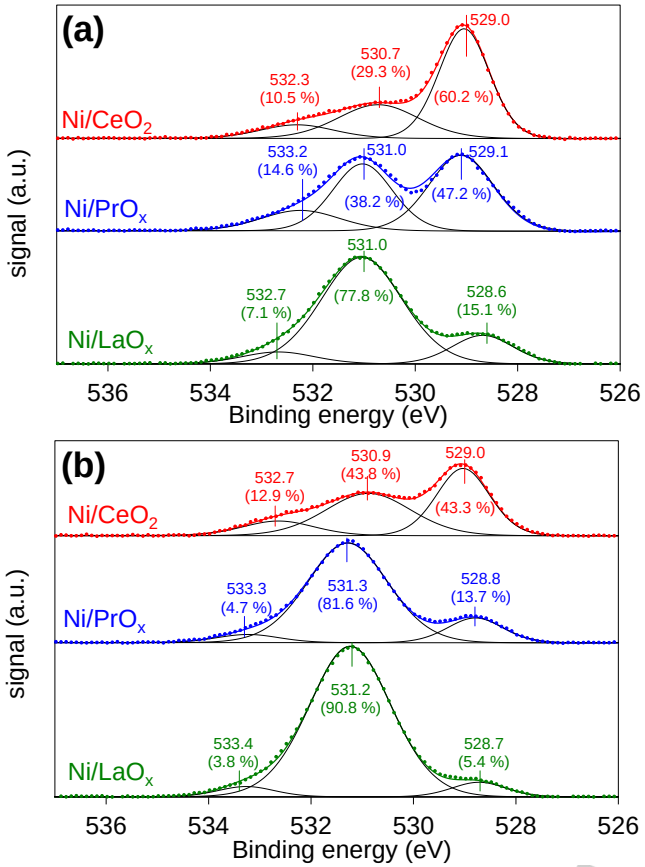


**Figure 7**. XPS characterization in the energy region of O1s transition for (a) fresh catalysts and (b) used catalysts.

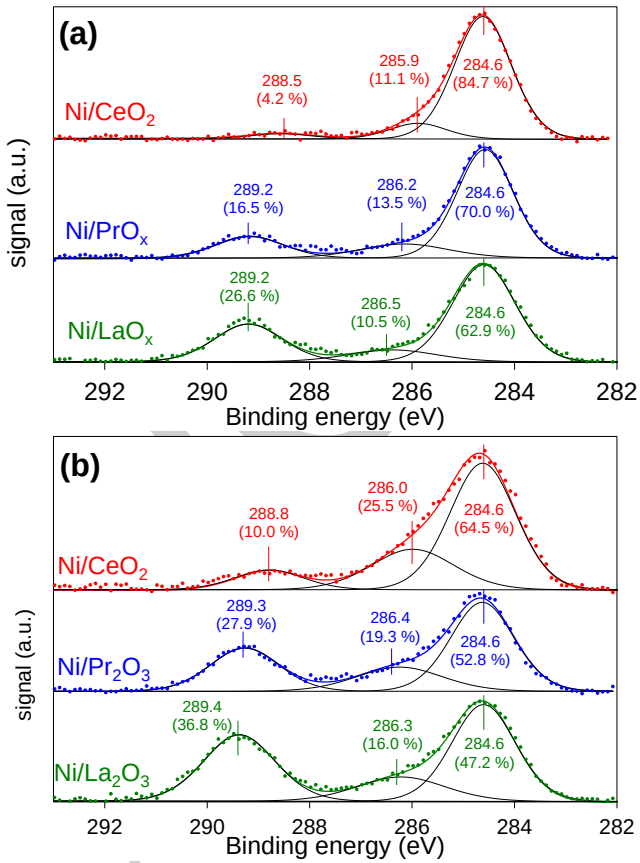


**Figure 8**. XPS characterization in the energy region of the C1s transition for (a) fresh catalysts and (b) used catalysts.

For fresh catalysts, the contribution to the total area of the O1s spectra of the band at 529 eV follows the trend $Ni/CeO_2$ > Ni/PrOx > Ni/LaOx, which is coincident with the catalytic activity trend (see Figure 5). The area of this band decreases after reaction for all catalysts, but the decrease is very relevant for Ni/PrOx (from 47.2 to 13.7 %) and Ni/LaOx (from 15.1 to 5.4 %), while not so remarkable for $Ni/CeO_2$ (from 60.2 to 43.3 %). These experimental observations suggest that the catalytic activity of the Ni/LnOx catalysts is in somehow related with the presence of a particular type of oxygen that is bounded to metal cations. These cations are probably $Ni^{2+}$ cations in close contact with the metal oxide support, that is, they are probably located at the nickel-support interface. Among the catalysts studied, this nickel-support synergy is more efficient for $Ni/CeO_2$ than for the other two catalysts.

In conclusion, considering the Ni2p and O1s spectra, we suggest that $Ni/CeO_2$ combines very electronegative reduced nickel sites suitable for $H_2$ dissociation with a $Ni^{2+}$-ceria interface very efficient for $CO_2$ dissociation.

Finally, the XPS spectra were analyzed in the C1s region, and the spectra for the fresh and used catalysts are compiled in Figure 8.

Three bands are also identified in the deconvoluted C1s spectra. Assignation of these bands is neither easy, but interesting information about the behavior of the catalysts during the methanation tests can be obtained from the band around 289 eV. This band increases for all catalysts during reaction, which is probably related in somehow with $CO_2$ chemisorption or with carbon intermediates. Both for fresh and used catalysts, the area of this band follows the opposite trend (Ni/LaOx > Ni/PrOx > $Ni/CeO_2$) than the catalytic activity, that is, the presence of stable carbon species on the catalysts surface is negative for the catalytic activity, probably because these carbon species block active sites and hinder the chemisorption of reactants. This observation is in agreement with the conclusions of the $N_2$-TPD characterization (Figure 3a).

As a summary, the activity for $CO_2$ methanation of the Ni/LnOx catalysts studied depends both on the nature of the catalytic active sites ($Ni^{2+}$ cations with strong interaction with the support and $Ni^0$) and on the stability of the $CO_2$ and $H_2O$ surface species, both variables being strongly affected by the LnOx support. $Ni/CeO_2$ is the best catalyst for $CO_2$ methanation for several reasons: i) the $Ni^{2+}$-ceria interaction leads to the formation of the highest population of active sites for $CO_2$ dissociation, ii) the reduced $Ni^0$ sites where $H_2$ dissociation takes place are the most electronegative and iii) this catalyst shows the lowest affinity for $CO_2$ and $H_2O$, keeping clean the catalyst surface during the

reaction. On the contrary, Ni/LaOx shows the lower activity because strongly chemisorbs $H_2O$ and $CO_2$, and because is not able to favor the formation of highly active sites for $CO_2$ and $H_2$ dissociation. The behavior of Ni/PrOx is slightly lower to that of $Ni/CeO_2$ because the formation of active sites is not so efficient and because the stability of $CO_2$ on surface is slightly higher. Note that both Ce and Pr can adopt the 3+ and 4+ oxidation states, and therefore can participate in the redox processes occurring at the $Ni^{2+}$-support interface during the catalytic tests, while La can only adopt the 3+ state, and therefore, is not expected to participate in these redox processes.

## Conclusions

Nickel catalysts with LaOx, $CeO_2$ and PrOx supports have been prepared, characterized and tested for $CO_2$ methanation, and the main conclusions of the study can be summarized as follows.

The nature of the nickel species present on fresh catalysts strongly depends on the support. The $Ni/CeO_2$ catalyst consists of a mixture of NiO and $CeO_2$ nanoparticles with comparable average crystallite sizes (22 and 30 nm, respectively) and a few fraction of nickel cations inserted into the $CeO_2$ lattice. Much smaller nickel oxide particles are dispersed on PrOx, without insertion of nickel cations into the PrOx lattices, and LaOx forms Ni-La mixed oxides and probably dispersed nickel oxide nanoparticles are also present on Ni/LaOx.

The catalytic activity for $CO_2$ methanation follows the trend $Ni/CeO_2$ (T50=300 ºC) > Ni/PrOx (T50=312 ºC) >> Ni/LaOx (T50=365 ºC), all catalysts being very selective towards $CH_4$ formation, and the activity depends both on the nature of the catalytic active sites and on the stability of the surface $CO_2$ and $H_2O$ species.

$Ni/CeO_2$ is the most active catalyst because the $Ni^{2+}$-ceria interaction leads to the formation of the highest population of active sites for $CO_2$ dissociation, the reduced $Ni^0$ sites where $H_2$ dissociation takes place are the most electronegative, and shows the lowest stability of surface $CO_2$ and $H_2O$ species.

The activity of Ni/PrOx is slightly lower to that of $Ni/CeO_2$ because the formation of active sites is not so efficient and because the stability of chemisorbed $CO_2$ is slightly higher.

Ni/LaOx shows the lowest activity because suffers strong chemisorption of $H_2O$ and $CO_2$, poisoning the catalyst surface, and because is not able to promote the formation of highly active sites for $CO_2$ and $H_2$ dissociation.

## Experimental Section

3.1. Catalysts preparation.

Three catalysts have been prepared, which are referred to as Ni/LaOx, $Ni/CeO_2$ and Ni/PrOx. The metal precursors used were $La(NO_3)_3{\cdot}6H_2O$ (Aldrich; 99.99%), $Ce(NO_3)_3{\cdot}6H_2O$ (Aldrich; 99%), $Pr(NO_3)_3{\cdot}6H_2O$ (Aldrich; 99.9%), and $Ni(NO_3)_2{\cdot}6H_2O$ (Aldrich; 98.5 %). The lanthanide oxide supports were prepared dissolving the metal precursors in ethanol (0.476 M) and citric acid was added to force the precipitation of metal citrates. After filtering, the solids were calcined at 600 ºC for 6 hours using a heating rate of 1 ºC $min^{-1}{\cdot}s$.

Ni was loaded by excess solvent impregnation using an ethanol solution of the nickel precursor with the required amount of salt to achieve a Ni loading of 10 wt. % on the catalysts. After total evaporation of the solvent, the solid was dried at 80 ºC overnight and calcined at 500 ºC for 2 hours with a heating rate of 5 ºC/min.

3.2. Catalysts characterization.

The porosity of the catalysts was studied by $N_2$ physisorption. $N_2$ isotherms were measured at -196 ºC in an automatic volumetric system (Autosorb-6, Quantachrome). The catalysts were outgassed at 150 ºC for 2 hours under vacuum before the adsorption.

X-Ray diffractograms were recorded in a Bruker D8 advance diffractometer, using a CuKα radiation source, a step of 0.02º and a time per step of 3 s.

Micro-XRF measurements were performed in an Orbis Micro-XRF Analyzer from EDAX. Areas of 300 µm in diameter were analyzed and three different spots were measured and averaged to obtain the mean composition of each catalyst.

The reduction of the fresh catalysts was studied by temperature programmed reduction with $H_2$ ($H_2$-TPR) and the accumulation of $CO_2$ and $H_2O$ by temperature programmed desorption in $N_2$ ($N_2$-TPD). The experiments were performed in a TG-MS device, with a thermobalance (Mettler Toledo; TGA/SDTA851) coupled to a mass spectrometer (Pfeiffer Vacuum; Thermostar GSD301T). 20 mg of fresh catalysts were heated in 5% $H_2$/Ar ($H_2$-TPR) or pure $N_2$ ($N_2$-TPD) flows (40 ml/min) at 10 ºC/min from room temperature until 900 ºC without previous pretreatment. A CuO reference sample was used to correlate the area under the $H_2O$ peaks in $H_2$-TPR experiments with the moles of $H_2$ consumed, and quantitative calculations have been performed. The m/z 18 ($H_2O$) has been used instead of m/z 2 ($H_2$) to follow the $H_2$-TPR experiments because peaks are better defined.

The surface of the catalysts was characterized by XPS in a K-ALPHA Thermo Scientific device. This device works with Al-Kα radiation (1486.6 eV) and includes a twin crystal monochromator, yielding a focused X-ray spot with a diameter of 400 µm, at 3 mA × 12 kV. The binding energy scale was adjusted by setting the C1s transition at 284.6 eV. The catalysts were characterized by XPS before and after the catalytic tests.

3.3. Catalytic tests.

$CO_2$ methanation tests were performed in a cylindrical fixed-bed reactor (9 mm inside diameter) coupled to a gas chromatograph (Agilent HP7890B). The catalyst was pre-treated at 500 ºC for 1 hour under 20%$H_2$/He flow (200 $cm^3{\cdot}min^{-1}$) for nickel oxide reduction, and after cooling to 200 ºC in inert gas, the reaction mixture was feed to the reactor, which consists of 16% $CO_2$ + 64% $H_2$ with He balance (total flow 200 $mL{\cdot}min^{-1}$). The temperature was increased from 200 to 450 ºC with a heating rate of 5 ºC/min, in steps of 25 ºC. Once the steady state was reached at every temperature step, the concentration of reactants and products at the reactor exit is determined by chromatographic analysis. Once the catalytic tests were finished at 450ºC, the reaction gas mixture was replaced by inert gas, the reactor was cooled down, the used catalysts were stored without control of the atmosphere, and were finally characterised by XPS.

The experiments were performed at atmospheric pressure with 0.4 grams of catalysts, which were pelletized, grinded and sieved, working with particles size between 300 and 500 µm. The catalyst particles were diluted with quartz particles (1-1.25 mm) up to ca. 1 $cm^3$ of bed, to improve mass and heat transfer. In these conditions, the GHSV was 12000 $h^{-1}$.

## Acknowledgements

The authors thank the financial support of Basque Government (Consolidated Group IT657-13), Spanish Ministry of Economy and Competitiveness (Projects CTQ2015-67597-C2-1-R and CTQ2015-67597-C2-2-R), and the EU (FEDER funding). ADQ thanks the Spanish Ministry of Education, Culture and Sports (grant FPU14/01178) and AQ the University of the Basque Country (grant PIF15/351).

**Keywords:** carbon dioxide; methane; nickel catalysts; hydrogenation; ceria; lanthanides

[1] T. Van Herwijnen, H. Van Doesburg, W.A. De Jong, J. Catal. **1973**, *28(3),* 391-402.
[2] B.A.Sexton; G.A.Somorjai. J. Catal. **1977**, *46 (2)*, 167-189.
[3] R. Maatman, S. A. Hiemstra, J. Catal. **1980**, *62(2)*, 349-356.
[4] F. Solymosi, A. Erdöhelyi, T. Bánsági, J. Catal. **1981**, *68(2),* 371-382.
[5] T. Yoshida, K. Nishizawa, M. Tabata, H. Abe, K. Hiroshi, T. Tatsuya, M. Tsuji, Y. Tamaura, J. Mater. Sci. **1993**, *28(5)*, 1220-1226.
[6] J.-N. Park, E.W. McFarland, J. Catal. **2009**, *266(1)*, 92-97.
[7] T. Abe, M. Tanizawa, K. Watanabe, A. Taguchi, Energy Environ. Sci. **2009**, *2(3)*, 315-321.
[8] S.K. Hoekman, A. Broch, C. Robbins, R. Purcell, Int. J. Greenhouse Gas Control **2010**, *4(1)*, 44-50.
[9] S. Sharma, Z. Hu, P. Zhang, E.W. McFarland, H. Metiu, J. Catal. **2011**, *278(2)*, 297-309.
[10] S. Tada, T. Shimizu, H. Kameyama, T. Haneda, R. Kikuchi, Int. J. Hydrogen Energy **2012**, *37(7)*, 5527-5531.
[11] P.A. U. Aldana, F. Ocampo, K. Kobl, B. Louis, F. Thibault-Starzyk, M. Daturi, P. Bazin, S.Thomas, A.C. Roger. Catal. Today **2013**, *215*, 201-207.
[12] M.A.A. Aziz, A.A. Jalil, S. Triwahyono, R.R. Mukti, Y.H. Taufiq-Yap , M.R. Sazegar. Appl. Catal., B **2014**, *147*, 359–368.
[13] J.C. Matsubu, V.N. Yang, P. Christopher, J. Am. Chem. Soc. **2015**, *137(8)*, 3076-3084.
[14] F. Wang, S. He, H. Chen, B. Wang, L. Zheng, M. Wei, D. G. Evans, X. Duan. J. Am. Chem. Soc. **2016**, *138(19)*, 6298-6305.
[15] K. Ray, G. Deo, Appl. Catal., B **2017**, *218,* 525-537.
[16] J.D. Holladay, J. Hu, D.L. King, Y. Wang. Catal. Today **2009**, *139*, 244–260.
[17] G. Gahleitner. Int. J. Hydrogen Energy **2013**, *38* 2039- 2061.
[18] H. Ahmad, S.K. Kamarudin, L.J. Minggu, M. Kassim, Renewable Sustainable Energy Rev. **2015**, *43,* 599-610.
[19] T. He, P. Pachfule, H. Wu, Q. Xu, P. Chen, Nat. Rev. Mater. **2016**, *1(12)*, 16059-16076.
[20] H. Hashimoto, M. Yamasaki, S. Meguro, T. Sasaki, H. Katagiri, K. Izumiya, N. Kumagai, H. Habazaki, E. Akiyama, K. Asami. Corros. Sci. **2002**, *44*, 371-386.
[21] N.M. Gupta, V.S. Kamble, K.A. Rao, R.M. Iyer, J. Catal. **1979**, *60(1)*, 57-67.
[22] F. Solymosi, A. Erdöhelyi, M. Kocsis, J. Chem. Soc., Faraday Trans. 1 **1981**, *77(5)*, 1003-1012.
[23] S. Scirè, C. Crisafulli, R. Maggiore, S. Minicò, S. Galvagno, Catal. Lett. **1998**, *51(3-4),* 41-45.
[24] T. Abe, M. Tanizawa, K. Watanabe, A. Taguchi, Energy Environ. Sci. **2009**, *2(3)*, 315-321.
[25] Q. Lin, X.Y. Liu, Y. Jiang, Y. Wang, Y. Huang, T. Zhang, Catal. Sci. Technol. **2004**, *4(7)*, 2058-2063.
[26] C. Janke, M. S. Duyar, M. Hoskins, R. Farrauto, Appl. Catal., B **2004**, *152-153(1)*, 184-191.
[27] D.C. Upham, A.R. Derk, S. Sharma, H. Metiu, E.W. McFarland, Catal. Sci. Technol. **2015**, *5(3)*, 1783-1791.
[28] Dreyer, J.A.H., Li, P., Zhang, L., Beh, G.K., Zhang, R., Sit, P.H.-L., Teoh, W.Y. Appl. Catal., B **2017**, *219*, 715-726.
[29] A. Erdöhelyi, M. Pásztor, F. Solymosi, J. Catal. **1986**, *98(1)*, 166-177.
[30] A. Karelovic, P. Ruiz, ACS Catal. **2013**, *3(12)*, 2799-2812.
[31] X. Wang, H. Shi, J.H. Kwak, J. Szanyi, ACS Catal. **2015**, *5(11)*, 6337-6349.
[32] Z. Zhang, A. Kladi, X.E. Verykios, J. Catal. **1994**, *148(2)*, 737-747.
[33] C. De Leitenburg, A. Trovarelli, J. Kašpar, J. Catal. **1997**, *166(1)*, 98-107.
[34] M. Jacquemin, A. Beuls, P. Ruiz, Catal. Today **2010**, *157(1-4)*, 462-466.
[35] A. Karelovic, P. Ruiz, J. Catal. **2013**, *301*, 141-153.
[36] S. Fujita, H. Terunuma, M. Nakamura, N. Takezawa. Ind. Eng. Chem. Res. **1991**, *30*, 1146-1151.
[37] A.E. Aksoylu, A.N. Akin, Z.I. Önsan, D.L. Trimm. Appl. Catal., A **1996**, *145(1-2)*, 185-193.
[38] M. Yamasaki, H. Habazaki, T. Yoshida, E. Akiyama, A. Kawashima, K. Asami, K. Hashimoto, M. Komori, K. Shimamura. Appl. Catal., A **1997**, *163(1-2)*, 187-197.
[39] Q. Pan, J. Peng, T. Sun, S. Wang, S. Wang, Catal. Commun. **2014**, *45*, 74-78.
[40] R.A. Hubble, J.Y. Lim, J.S. Dennis. Faraday Discuss. **2016**, *192*, 529-544.
[41] L. Xu, F. Wang, M. Chen, J. Zhang, K. Yuan, L. Wang, K. Wu, G. Xu, W. Chen, RSC Adv. **2016**, *6(34)*, 28489-28499.
[42] L. Xu, F. Wang, M. Chen, D.Y. Nie X.B. Lian Z.Y. Lu, H.X.Chen, K. Zhang, P. Ge, Int. J. Hydrogen Energy **2017**, *42(23)*, 15523-15539.
[43] P. Frontera, A. Macario, M. Ferraro, P. L. Antonucci. Catalysts **2017**, *7,* 59-87.
[44] S. Huanling, Y. Jian, Z. Jun, C. Lingjun. Chin. J. Catal. **2010**, *31*, 21–23.
[45] G. Zhi, X. Guo, Y. Wang, G. Jin, X. Guo. Catal. Commun. **2011**, *16,* 56-59.
[46] D.J. Kim, J. Am. Ceram. Soc. **1989**, *72*, 1415–1421.
[47] M. Mogensen, in: A. Trovarelli (Ed.), Catalysis by Ceria and Related Materials, Imperial College Press, London, 2002, p. 462.
[48] S. C. Bradwell, A. Kapusta, S. J. Milne. J. Mater. Chem., **1991**, *1(5)*, 891-892.
[49] S. Bernal, F. J. Botana, R. Garcia, F. Ramirez, J. M. Rodríguez-Izquierdo. J. Mater. Sci. **1987**, *22(10)*, 3793-3800.
[50] S. Bernal, F.J. Botana, R. García, F. Ramírez, J.M. Rodríguez-Izquierdo, J. Chem. Soc., Faraday Trans. 1 **1987**, *83(8)*, 2279-2287.
[51] G.L. Markaryan, L.N. Ikryannikova, G.P. Muravieva, A.O. Turakulova, B.G. Kostyuk, E.V. Lunina, V.V. Lunin, E. Zhilinskaya, A. Aboukais. Colloids Surf., A **1999**, *151*, 435-447.
[52] F. Fally, V. Perrichon, H. Vidal, J. Kaspar, G. Blanco, J.M. Pintado, S. Bernal, G. Colon, M. Daturi, J.C. Lavalley. Catal. Today **2000**, *59*, 373–386.
[53] B. Miao, S. S. Khine Ma, X. Wang, H. Su, S. Hwa Chan. Catal. Sci. Technol. **2016**, *6*, 4048-4058.
[54] A. Caballero, J. P. Holgado, V. M. Gonzalez-de la Cruz, S. E. Habas, T. Herranz, M. Salmeron. Chem. Commun., **2010**, *46*, 1097–1099.
[55] H. Li, H. Li, W.-L. Dai, W. Wang, Z. Fang, J.-F. Deng. Appl. Surf. Sci. **1999**, *152*, 25–34.
[56] Z. Hou, O. Yokota, T. Tanaka, T. Yashima. Appl. Catal., A **2003**, *253*, 381–387.

[57] E. Heracleous, A.F. Lee, K. Wilson, A.A. Lemonidou. J. Catal. 231 (2005) 159–171.

[58] J. Kugai, V. Subramani, C. Song, M. H. Engelhard, Y.-H. Chin. J. Catal. **2006**, *238,* 430–440.

10.1002/cctc.201801585

WILEY-VCH



# FULL PAPER

$Ni/CeO_2$ is the most active Ni/LnOx catalyst because (i) the $Ni^{2+}$-ceria interaction leads to the formation of the highest population of active sites for $CO_2$ dissociation, (ii) the reduced $Ni^0$ sites where $H_2$ dissociation takes place are the most electronegative and active, and (iii) the stability of surface $CO_2$ and $H_2O$ species is lowest.

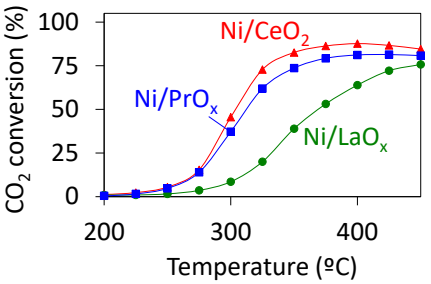


*Virginia Alcalde-Santiago, Arantxa Davó-Quiñonero, Dolores Lozano-Castelló, Adrián Quindimil, Unai De-La-Torre, Beñat Pereda-Ayo, José A. González-Marcos, Juan R. González-Velasco, Agustín Bueno-López**

***Page No. – Page No.***

**Ni/LnOx catalysts (Ln = La, Ce or Pr) for $CO_2$ methanation**